SUBCONTRACT TITLE: IDENTIFYING THE ELECTRONIC PROPERTIES RELEVANT TO IMPROVING THE PERFORMANCE OF HIGH BAND-GAP COPPER BASED I-III-$V1_2$ CHALCOPYRITE THIN FILM PHOTOVOLTAIC DEVICES

SUBCONTRACT NO: XAT-4-33624-08

QUARTERLY TECHNICAL STATUS REPORT FOR: Phase I/Quarter 1
27 April 2004 to 26 July 2004

SUBMITTED TO: Martha Symko-Davies
National Renewable Energy Laboratory

PRINCIPAL INVESTIGATOR: J. David Cohen, Department of Physics
University of Oregon, Eugene, OR 97403
2nd Tier Subcontractor : Jennifer T. Heath, Department of Physic
Linfield College, McMinnville, OR 97128

This report covers the first quarter of Phase I for the period April 27,2004 to July 26, 2004, of the Phase IB High Performance PV Subcontract XAT-4-33624-08. The work to be reported during this period is primarily related to the development and evaluation of additional experimental techniques (Task 4). Specifically, as a prelude toward applying modulated photocurrent (MPC) methods to the higher bandgap CIS alloys in hopes of identifying minority carrier trapping processes, we have carried out high frequency admittance measurements of CIGS samples to measure the dielectric relaxation times as a function of temperature. These measurements have turned out to be valuable in themselves, since they have allowed us to determine the hole carrier mobilities directly in working CIGS solar cell devices.

Hole mobilities in both epitaxial and polycrystalline CIGS materials have previously been determined in the traditional manner, using the Hall effect in conjunction with resistivity measurements. Such measurements require insulating substrates with coplanar contacts and thus cannot be performed on working solar cell devices. Morevoer, such devices employ CIGS layers that are comparable in thickness to the typical 1μm crystallite size; thus, it is not clear how relevant such Hall mobility measurements may be for understanding the cell carrier collection.

During the past quarter we have succeeded in demonstrating that the resistivity within the absorber layer of working CIGS cells can be determined using ac measurements. Taken together with the hole carrier densities deduced using our drive-level capacitance profiling (DLCP) method, this has enabled us to determine the hole mobilities in the CIGS layer within a working cell. The polycrystalline CIGS devices for our measurements were fabricated at the Institute of Energy Conversion at the University of Delaware. CIGS films were grown roughly 2 μm thick using four-source elemental evaporation. The film compositions, determined by energy dispersive x-ray spectroscopy, are slightly Cu poor, with Cu/(In+Ga)=0.8-0.9. Auger depth profiles indicate uniform Ga compositions. To form devices, a chemical bath was used to deposit 30-40 nm of CdS, then a 0.5μm thick layer of ZnO:Al was sputtered to form the top contact, with evaporated Ni/Al grids. In some samples, the ZnO:Al was replaced by a 50 nm ZnO layer followed by 0.2μm ITO.

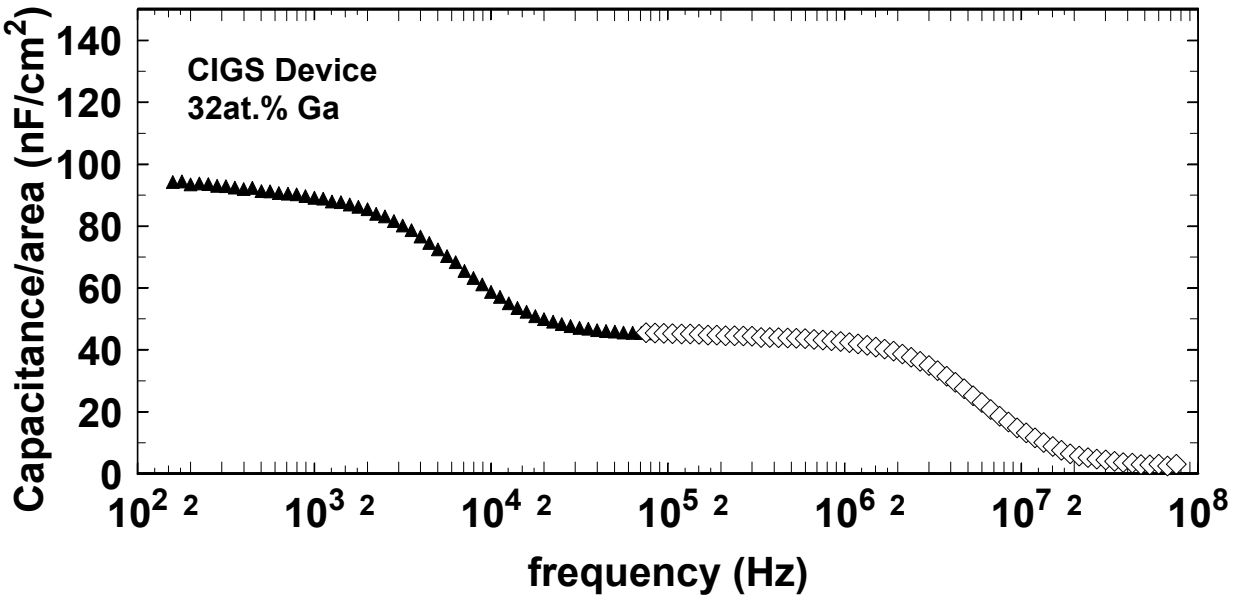

FIG. 1. Capacitance vs. frequency of CIGS solar cell obtained under 0V applied bias at 120K. The filled symbols were obtained using our standard low frequency capacitance bridge, and the open symbols were obtained using our newly implemented high frequency capacitance bridge and sample probe. Note the sharp decrease in capacitance above 3MHz corresponding to dielectric freeze out of the CIGS layer.

In Fig. 1 we display the results of applying both our standard capacitance measurements together with our newly implemented high frequency capacitance measurements on one such CIGS sample device. One clearly sees three regimes: (1) Frequencies, f, between about 10^4 and 10^6 Hz exhibit a nearly constant capacitance. This corresponds to the depletion capacitance of the CIGS sample junction, $C_d = \varepsilon A/W$, where W is the depletion width. (2) At frequencies below 10 kHz the capacitance increases and then reaches another higher plateau. This indicates the well-known additional response of deep defects within the depletion region. (3) Above 2MHz the capacitance decreases and reaches a much lower value. This is due to the dielectric carrier freeze out; i.e., where $1/f$ becomes shorter than the dielectric relaxation time $\rho\varepsilon$. This capacitance step can be clearly distinguished from other capacitance steps because, on the high frequency side of the step, the capacitance is *independent of applied bias* and approaches the geometric capacitance, $C_g \equiv \varepsilon A/t$, where A is the area and t is thickness of the film. In this high frequency regime the CIGS absorber essentially behaves as an *insulator* with dielectric constant $\varepsilon \approx 12\varepsilon_0$. Because the dielectric constant, ε, of CIGS is fairly well known, the identification of the dielectric relaxation time allows one to determine the resistivity of the undepleted portion of the CIGS film within the working device.

At frequencies higher than about 100kHz, the response of deeper states within the depletion region can be ignored. Thus we been able to model the device simply as a depletion capacitance, $C_d = \varepsilon A/W$ in series with the undepleted bulk region of the CIGS absorber. The latter may be treated as a series of slices of infinitesimal width, δx [such that $\Sigma\delta x = (t-W)$], each having a capacitance $c = \varepsilon A/\delta x$, in parallel with a resistance $r = \rho\, \delta x/A$. The equivalent circuit

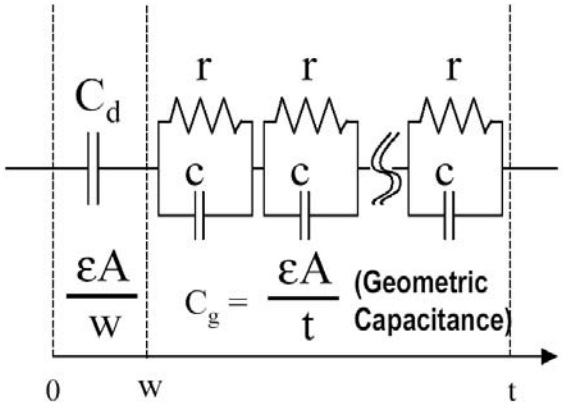

FIG. 2. Equivalent circuit employed to deduce the dielectric relaxation time, and hence the resistivity, of the CIGS absorber within a solar cell device. This circuit consists of the depletion capacitance, C_d, in series with an infinite series of *rc* parallel circuits, each corresponding to an infinitesimal width, δx, of the undepleted portion of the CIGS layer. The value of *rc* of each such element is then equal to $\rho\varepsilon$, the dielectric relaxation time.

for this analysis is shown in Fig. 2. Using this analysis we readily obtain expressions for the capacitance and conductive phases of the admittance response (here $\omega = 2\pi f$):

$$C = C_d \frac{1+(C_d/C_g)(\rho\varepsilon\,\omega)^2}{1+(C_d/C_g)^2(\rho\varepsilon\,\omega)^2} \qquad G/\omega = C_d \frac{[(C_d/C_g)-1](\rho\varepsilon\,\omega)}{1+(C_d/C_g)^2(\rho\varepsilon\,\omega)^2} \tag{1}$$

An example of using these to fit actual high frequency admittance data for one CIGS sample device is shown in Fig. 3. In fitting the data at –1V applied bias we found, as expected, that only the depletion capacitance C_d needed to be changed substantially, while the fitted value of $\rho\varepsilon$ remained the same (roughly 1.15 ns) within the statistical error. Assuming a dielectric constant of 11.7, this implies a resistivity of 1120 Ω-cm.

As a comparison test, IEC deposited one film (#444) both on bare glass and Mo coated glass (with the latter finished as a solar cell). We compared the ac determination of resistivity with that given by a standard (dc) 4-point probe measurement on the bare glass sample. For this sample the ac admittance method yielded 580 Ω-cm at 200K, while the 4-point probe gave 420 Ω-cm at room temperature. Given that the temperature dependence for conductivity in these samples appears very weak, we consider this agreement between the two methods to be good.

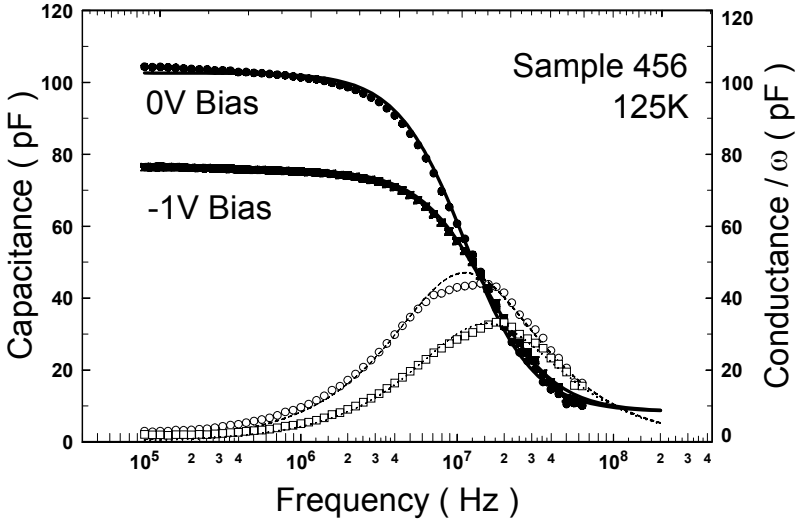

FIG. 3. High frequency capacitance (solid symbols) and conductance data (open symbols) on CIGS sample #456 at a temperature of 125K and two different values of applied bias. The lines through the data points indicate fits obtained using Eq. (1). Essentially identical values of $\rho\varepsilon$ were obtained for the two different DC biases.

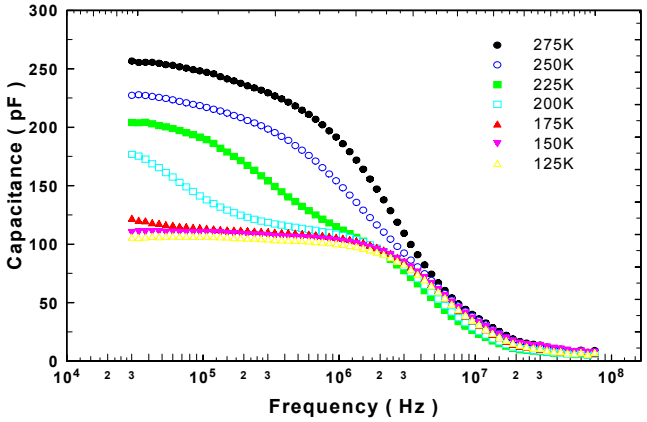

FIG. 4(a). High frequency admittance vs. temperature for the 27at.% Ga CIGS sample #456 under 0V applied bias.

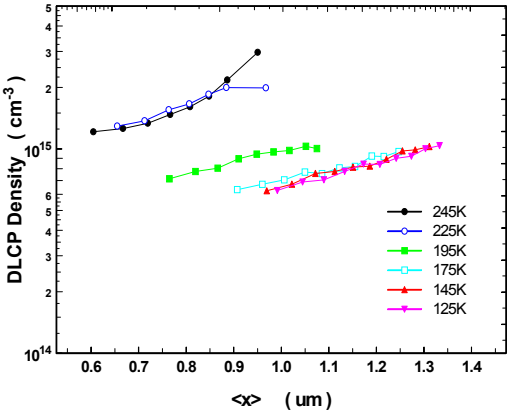

FIG.4(b) 1MHz DLCP profiles vs. $\langle x \rangle \equiv \varepsilon A/C_0$ for a similar range of temperatures as in (a). These data imply a hole mobility near 150K of 10±2 $cm^2V^{-1}s^{-1}$.

The hole carrier densities were found using the drive-level capacitance profiling (DLCP) method. At sufficiently high frequencies and/or low temperatures the deduced DLCP density should have little contribution from deep states and thus be dominated the hole carrier density, p. This should occur at frequencies just below the dielectric freeze out condition. However, in order for N_{DL} to reflect only the free carrier density close to freeze-out, it is important that the Fermi energy not be pinned at a region of high state density in the gap. Otherwise, even at freeze out, there may be a significant contribution to N_{DL} from such defects, resulting in an overestimate of the carrier density based upon this method. In Fig. 4 we display both the admittance and 1MHz DLCP data obtained at a series of measurement temperatures for the same CIGS sample as in Fig. 3. From Fig. 4(a) we see that 1MHz is indeed a reasonable choice since it lies well below the freeze-out regime that extends from about 3MHz to 20MHz. In Fig. 4(b) we see that, in fact, the value of N_{DL} is nearly independent of temperature between 125K and 175K, although it shows some spatial variation (less than a factor of 2 over 0.5μm). The N_{DL} profiles do appear to be indicative of the free hole carrier densities for this sample between 125K and 175K and, using the values of ρε deduced from Fig. 4(a), we deduce a nearly temperature independent hole mobility in this temperature range of 10±1.8 $cm^2V^{-1}s^{-1}$.

The major source of uncertainty in the determined mobility arises from the spatial variation in the free carrier density (the statistical uncertainty for this case is only ±0.4 $cm^2V^{-1}s^{-1}$). Above 175K the DLCP profile values increase and then reach a second plateau at about 245K. We can offer two possible explanations for this: Either a band of deeper states within the depletion region can respond at these higher temperatures and thus adds to the DLCP determined density, or the free hole carrier density actually increases as a band of deeper acceptors becomes fully ionized at these higher temperatures. For now we will restrict our estimates of the mobilities to the lower temperature regime (near 150K) where this issue does not arise. Results of hole mobilities determined for six CIGS samples using this method are listed in Table I. We see that the 150K hole mobilities vary by nearly an order of magnitude, from about 3 $cm^2V^{-1}s^{-1}$ to over 20 $cm^2V^{-1}s^{-1}$. These mobilities do not appear to be correlated in any obvious manner to the cell performance. All of the mobilities listed lie well within the range of Hall mobilities determined

TABLE I. Summary of samples and the hole mobilities determined by high frequency admittance measurements. Cell efficiencies for each device sample are included. The deduced values of ρε, and the hole carrier densities determined by DLCP, are also indicated.

Sample #	Ga (at.%)	Eff (%)	p (10^{14} cm^{-3})	ρε (ns)	μ_h (cm^2/Vs)
008	0	9.53	8.8 ± 0.6	2.5 ± 0.2	2.9 ± 0.3
456	27	11.6	11 ± 3	1.5 ± 0.1	3.9 ± 1.1
400	32	16.1	8.2 ± 0.5	1.1 ± 0.1	7.2 ± 0.8
233	32	14.3	5.9 ± 0.8	0.92 ± 0.1	12 ± 2.1
264	32	11.8	4.8 ± 1.1	0.77 ± 0.1	18 ± 4.0
444	34	12.3	5.0 ± 0.4	0.58 ± 0.1	22 ± 4.2

previously for polycrystalline CIGS samples, and about an order of magnitude lower than Hall mobilities determined for epitaxial CIGS films.

Finally, in an attempt to gain some insight into the mechanisms limiting the mobilities in such samples, we examined one sample over a series of metastable states. It has been now been well established that, in particular, the free hole carrier density can be increased significantly following long term light exposure, and that these changes anneal away within a few hours at room temperature. Exploiting such metastable effects, we measured both the high frequency admittance (10^5 to 10^8 Hz) and 1MHz DLCP profiles of one 32at.% Ga sample at 125K. We then light soaked this sample at room temperature using 780 nm monochromatic light at 100mW/cm^2 light intensity for 3 hours. It was then immediately cooled to 125K and re-measured. We found that both spectra changed significantly: the depletion capacitance increased by a factor of about 1.7 while the DLCP determined hole carrier density increased by roughly a factor of 2 [see Fig. 5]. However, the change in conductivity was by a much smaller factor, as indicated by the frequency of the dielectric freeze-out.

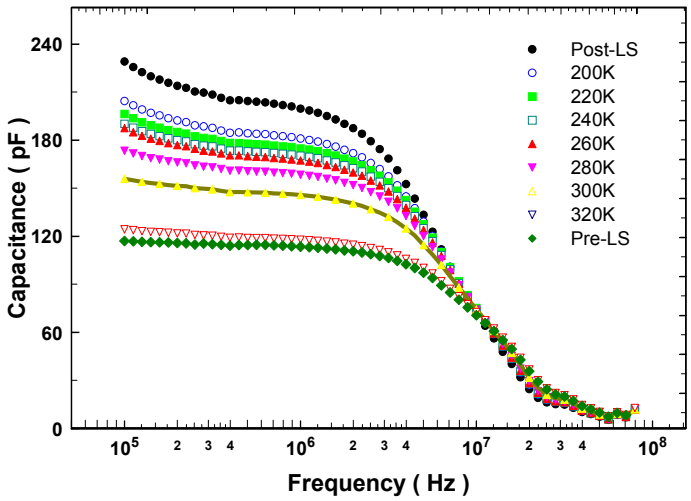

FIG. 5(a). Set of 125K admittance data at 0V applied bias for a sequence of metastable states of a 32at.% Ga CIGS sample (#400).

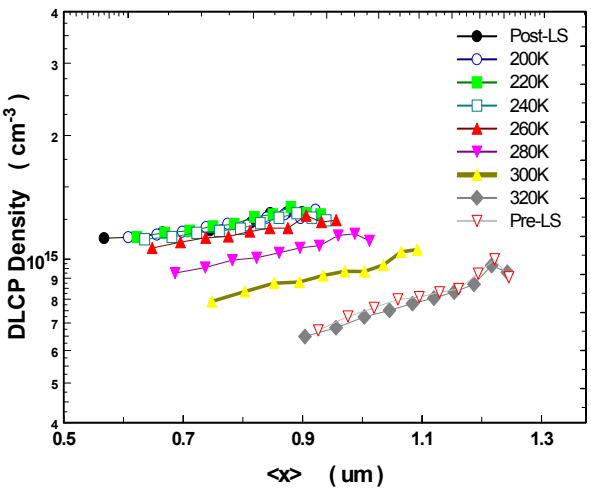

FIG.5(b) 1 MHz DLCP data for the same metastable states as in (a). The sequence of 10 min. anneal temperatures are indicated.

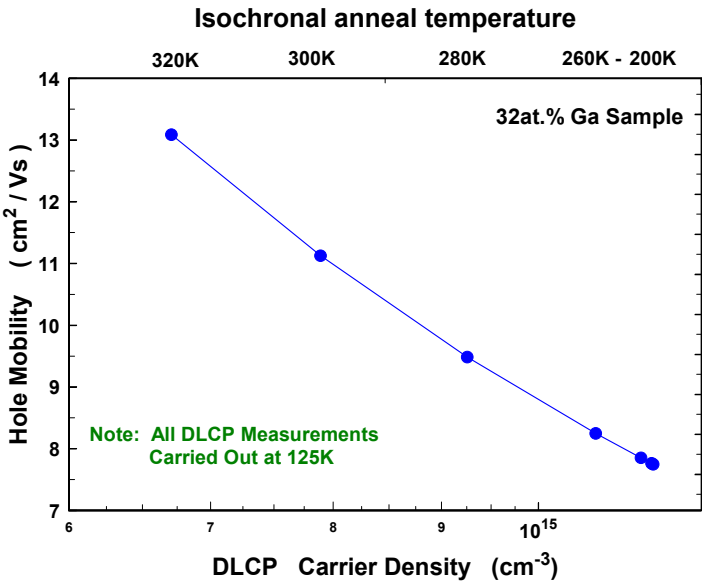

FIG. 6. Hole mobilities for the sequence of metastable states as derived from the data in Fig. 5. The inverse relation between the mobilities and carrier densities reflect the fact that the conductivity is nearly constant over this set of metastable states.

We next subjected the samples to a series of 10 minute isochronal anneals in the dark, beginning with 200K, increasing in 20K steps, until a 10 minute anneal at 320K had been completed. After each such anneal, the admittance and DLCP profiles were re-measured at 125K. Following the 320K anneal we found that the sample exhibited nearly the same characteristics as it had prior to light-soaking. These data are displayed in Fig. 5. Note that the admittance spectra exhibit a marked change even after the first (200K) anneal, while the DLCP curves do not change significantly until after the 260K anneal. We believe that the latter indicates the temperature at which the CIGS absorber properties begin to recover, while the changes in admittance seen at lower temperatures are restricted to changes in sample properties near the barrier junction (which effectively modify the built in potential and hence the depletion capacitance). The hole mobilities determined from these measurements are plotted in Fig. 6. The nearly inverse relationship between mobility and carrier density reflects the very small change in the deduced conductivities.

In summary, we believe we have amply demonstrated that high frequency admittance techniques can be used to obtain the resistivity of the undepleted region of the absorber in CIGS solar cells. Taken together with drive-level capacitance profiling measurements to determine the hole carrier densities, we are then able to estimate the hole mobilities directly within these working devices. This eliminates the need for depositing companion films on insulating substrates to examine the carrier mobility properties, at least over a restricted temperature range.

The experimental results reported above indicate fairly good agreement using this method as compared to coplanar measurements, but this is somewhat surprising. The lower carrier mobility in polycrystalline versus epitaxial CIGS films has been interpreted to imply the existence of potential barriers at grain boundaries that limit carrier transport. However, because the grains are typically 1μm in size, and comparable to the thickness of our films, we would not expect such grain boundary effects to play as significant a role. Thus, the agreement between the coplanar and sandwich measurements of resistivity was not really expected. Further measurements are underway to try to understand the implications of this result.